

University of Groningen

Biallelic loss-of-function variants in RABGAP1 cause a novel neurodevelopmental syndrome

Oh, Rachel Youjin; Deshwar, Ashish R.; Marwaha, Ashish; Sabha, Nesrin; Tropak, Michael; Hou, Huayun; Yuki, Kyoko E.; Wilson, Michael D.; Rump, Patrick; Luning, Roelineke

Published in:
Genetics in Medicine

DOI:
[10.1016/j.gim.2022.07.024](https://doi.org/10.1016/j.gim.2022.07.024)

IMPORTANT NOTE: You are advised to consult the publisher's version (publisher's PDF) if you wish to cite from it. Please check the document version below.

Document Version
Publisher's PDF, also known as Version of record

Publication date:
2022

[Link to publication in University of Groningen/UMCG research database](#)

Citation for published version (APA):

Oh, R. Y., Deshwar, A. R., Marwaha, A., Sabha, N., Tropak, M., Hou, H., Yuki, K. E., Wilson, M. D., Rump, P., Luning, R., Elserafy, N., Chung, C. W. T., Hewson, S., Klein-Rodewald, T., Calzada-Wack, J., Moreno, A. S., Kraiger, M., Marschall, S., Fuchs, H., ... Schulze, A. (2022). Biallelic loss-of-function variants in RABGAP1 cause a novel neurodevelopmental syndrome. *Genetics in Medicine*, 24(11), 2399-2407. <https://doi.org/10.1016/j.gim.2022.07.024>

Copyright

Other than for strictly personal use, it is not permitted to download or to forward/distribute the text or part of it without the consent of the author(s) and/or copyright holder(s), unless the work is under an open content license (like Creative Commons).

The publication may also be distributed here under the terms of Article 25fa of the Dutch Copyright Act, indicated by the "Taverne" license. More information can be found on the University of Groningen website: <https://www.rug.nl/library/open-access/self-archiving-pure/taverne-amendment>.

Take-down policy



If you believe that this document breaches copyright please contact us providing details, and we will remove access to the work immediately and investigate your claim.

Downloaded from the University of Groningen/UMCG research database (Pure): <http://www.rug.nl/research/portal>. For technical reasons the number of authors shown on this cover page is limited to 10 maximum.



BRIEF REPORT

Biallelic loss-of-function variants in *RABGAP1* cause a novel neurodevelopmental syndrome

Rachel Youjin Oh¹ , Ashish R. Deshwar^{1,2}, Ashish Marwaha³, Nesrin Sabha², Michael Tropak², Huayun Hou², Kyoko E. Yuki², Michael D. Wilson², Patrick Rump⁴, Roelineke Luning⁴, Noha Elserafy⁵, Clara W.T. Chung^{5,6}, Stacy Hewson¹, Tanja Klein-Rodewald⁷, Julia Calzada-Wack⁷, Adrián Sanz-Moreno⁷, Markus Kraiger⁷, Susan Marschall⁷, Helmut Fuchs⁷, Valerie Gailus-Durner⁷, Martin Hrabe de Angelis^{7,8,9}, James Dowling^{2,10}, Andreas Schulze^{1,2,11,*} 

ARTICLE INFO

Article history:

Received 6 June 2022

Received in revised form

25 July 2022

Accepted 26 July 2022

Available online 9 September 2022

Keywords:

Autosomal recessive

GTPase-activating protein

Neurodevelopmental syndrome

Novel Mendelian disorder

ABSTRACT

Purpose: *RABGAP1* is a GTPase-activating protein implicated in a variety of cellular and molecular processes, including mitosis, cell migration, vesicular trafficking, and mTOR signaling. There are no known Mendelian diseases caused by variants in *RABGAP1*.

Methods: Through GeneMatcher, we identified 5 patients from 3 unrelated families with homozygous variants in the *RABGAP1* gene found on exome sequencing. We established lymphoblastoid cells lines derived from an affected individual and her parents and performed RNA sequencing and functional studies. *Rabgap1* knockout mice were generated and phenotyped.

Results: We report 5 patients presenting with a common constellation of features, including global developmental delay/intellectual disability, microcephaly, bilateral sensorineural hearing loss, and seizures, as well as overlapping dysmorphic features. Neuroimaging revealed common features, including delayed myelination, white matter volume loss, ventriculomegaly, and thinning of the corpus callosum. Functional analysis of patient cells revealed downregulated mTOR signaling and abnormal localization of early endosomes and lysosomes. *Rabgap1* knockout mice exhibited several features in common with the patient cohort, including microcephaly, thinning of the corpus callosum, and ventriculomegaly.

Conclusion: Collectively, our results provide evidence of a novel neurodevelopmental syndrome caused by biallelic loss-of-function variants in *RABGAP1*.

© 2022 American College of Medical Genetics and Genomics.

Published by Elsevier Inc. All rights reserved.

Introduction

RABGAP1 (also termed as GAPCenA, TBC1D11, or Rab GTPase-activating protein 1) is a GTPase-activating protein

that has been found to interact with many different RAB GTPase proteins, including RAB6A, RAB6B, RAB2, RAB4, and RAB36.^{1–3} *RABGAP1* consists of an N-terminal phosphotyrosine interaction domain, a conserved catalytic

Rachel Youjin Oh and Ashish R. Deshwar contributed equally.

*Correspondence and requests for materials should be addressed to Andreas Schulze, The Hospital for Sick Children, 555 University Avenue, Toronto, Ontario, Canada M5G 1X8. E-mail address: andreas.schulze@sickkids.ca

Affiliations are at the end of the document.

doi: <https://doi.org/10.1016/j.gim.2022.07.024>

1098-3600/© 2022 American College of Medical Genetics and Genomics. Published by Elsevier Inc. All rights reserved.

TBC (TRE2/BUB2/CDC16) domain, which promotes guanosine triphosphate hydrolysis, and a C-terminal coiled-coil domain.^{1,3,4} It has been implicated in a diverse number of cellular processes, including endosomal trafficking, mitosis, and cell migration.^{1,5-10} RABGAP1 has also been shown to modulate intracellular lysosomal positioning and vesicular trafficking to promote mTOR complex 1 (mTORC1) signaling, a critical pathway in cell proliferation and growth.¹¹ No pathogenic variants in *RABGAP1* have been reported in association with human diseases.

We report in this article 5 affected individuals from 3 unrelated families presenting with a spectrum of neurodevelopmental abnormalities, including global developmental delay/intellectual disability, microcephaly, bilateral sensorineural hearing loss, seizures, overlapping dysmorphic features, and brain anomalies, including ventriculomegaly and thinning of the corpus callosum. Homozygous predicted loss-of-function (LOF) variants in the *RABGAP1* gene were identified in all 5 individuals through exome sequencing (ES). Functional studies using patient cells revealed a reduction in mTOR signaling and abnormal positioning of lysosomes and early endosomes, consistent with loss of RABGAP1 function. Finally, a mouse knockout of *Rabgap1* was found to have similar brain anomalies, including thinning of the corpus callosum and ventriculomegaly. Altogether, we provide evidence of a novel neurodevelopmental syndrome caused by biallelic LOF variants in *RABGAP1*.

Materials and Methods

RABGAP1 variants were discovered through ES after clinical evaluation. Contact between clinicians and researchers was mediated by GeneDx/GeneMatcher. Informed consent was obtained for all participants for publication.

Detection and quantification of *RABGAP* exon 4/5 splicing levels using quantitative polymerase chain reaction

Levels of RABGAP, RABGAPL1, and TBP exon pairs were detected/quantified using quantitative polymerase chain reaction (qPCR) after first strand complementary DNA (cDNA) synthesis using total RNA extracted from proband (patient 1), parental, and control unaffected patient lymphoblastic cell lines (LCLs). cDNA was prepared from 1 μ g of total RNA from each of the patient samples listed earlier, using SuperScript IV VILO Master Mix (Thermo Fisher Scientific) as per manufacturers protocol in a total of volume of 20 μ L.

To detect the expected altered splicing between exons 4 and 5 in the proband, 1 μ L of a 10-fold dilution of the cDNA reaction was used in PCR consisting of MyTaq HS Mix 2X (Froggabo) and 1 μ L of RABGAP1Ex4F and RABGAP1Ex5R primers (50 ng/ μ L) in a total volume of 50 μ L using

the following amplification cycle, 95 °C for 2 minutes followed by 40 cycles of 95 °C for 20 seconds, 58 °C for 20 seconds, and 72 °C for 30 seconds. PCR products were resolved using Tris, acetate, and EDTA gel electrophoresis on a 2% agarose gel.

For real-time qPCR of RABGAP exon pairs, patient cDNA samples were diluted 10-fold. PCR mixtures consisted of 3 μ L diluted cDNA mixture, 0.5 μ L of 50 ng/ μ L forward and reverse primers, distilled water, and 5 μ L of iQ SYBR Green Supermix (Bio-Rad). Amplification was performed on a CFX96 Touch Real Time qPCR machine (BioRad) using the following cycle program 95 °C for 5 minutes, 40 cycles of 95 °C for 15 seconds, 52 °C for 15 seconds annealing, and 72 °C for 15 seconds extension step. RABGAP and RABGAPL1 exon pairs were normalized to TBP and relative to their respective target genes in the control unaffected patient samples using 2(- $\Delta\Delta$ CT) method (see [Supplemental Materials and Methods](#) for primers used for amplification of target exon pairs).

RNA sequencing

RNA was extracted from LCLs using an RNeasy Kit (Qiagen) and quality was determined using TapeStation RNA ScreenTape (Agilent). A total of 250 ng of RNA spiked with SIRV Set 3 (Lexogen) was enriched for poly(A) and libraries were prepared using an automated NEBNext Poly(A) mRNA Magnetic Isolation Module and NEBNext Ultra II Directional RNA Library Prep kit for Illumina (NEB) on the NGS Workstation (Agilent). Libraries were analyzed for quality using TapeStation High Sensitivity DNA ScreenTape (Agilent) and quantified using KAPA library quantification (Roche) before sequencing on a Nova-Seq 6000 System (Illumina).

RNA sequencing analysis

Raw sequencing reads were aligned to a hybrid genome of hg19 (1000 Genomes reference genome, hs37d5) and the spike-in sequences (SIRVome, SIRV set3) using Spliced Transcripts Alignment to a Reference (v2.6.1c). Gene annotation was obtained from Ensembl (v75) and combined with SIRVome transcript annotation. Gene expression level quantification was performed using RNA-Seq by Expectation Maximization (v1.2.22). Splicing junctions were visualized using the Integrated Genomics Viewer.

Cell culture

Human LCLs were generated from patient 1 and her mother and father at the The Centre for Applied Genomics (TCAG) at the Hospital for Sick Children. A separate healthy control was also used. Lymphoblastoid suspension cells were cultured in RPMI-1640 (Wisent Bioproducts) supplemented with 15% fetal bovine serum (Wisent Bioproducts) and 1%

antibiotics (Wisent Bioproducts). Cells were grown in a humidified atmosphere with 5% carbon dioxide at 37 °C.

Immunofluorescence

Lymphoblastoid suspension cells were seeded on cover slips treated with 0.01% polylysine (ThermoFisher Scientific). For indirect immunofluorescence, cells were fixed in ice-cold 4% paraformaldehyde for 15 minutes at room temperature, blocked for 1 hour, then incubated overnight at 4 °C with antibodies to LAMP2 (DSHB, H4B4, lysosomal marker) and RAB5 (abcam ab66746, early endosomal marker) diluted at 1:100 dilution in blocking solution. Secondary antibodies (Alexa Fluor 488; Invitrogen) were applied for 1 hour at room temperature at 1:1000 dilution. Micrographs were captured with an Infinity1 camera (Lumenera Corp) through an Olympus BX43 light microscope. Quantification was performed manually using ImageJ from Ki67, Lamp2 and Rab5 immunofluorescence images taken at 60× magnification.

Immunoblotting

LCL protein lysates (30 µg/lane) were resolved through sodium dodecyl sulfate-polyacrylamide gel electrophoresis, and proteins were transferred onto polyvinylidene fluoride membranes, according to standard procedures. Membranes were blocked in 5% skim milk powder and 3% bovine serum albumin and incubated overnight with primary antibody. Primary antibodies used were pAKT (1:1000, Cell Signaling Technology, 4060), AKT (1:1000, Cell Signaling Technology, 9272), pS6 (1:1000, Cell Signaling Technology, 9205), Total S6 (1:1000, Cell Signaling Technology, 9202), and HSP90 (1:1000, Origene, TA500494). After extensive washing, membranes were incubated for 1 hour with horseradish peroxidase-conjugated goat antirabbit secondary antibody (1:5000, BioRad) in 5% skim milk powder and 3% bovine serum albumin.

Rabgap1 mouse model generation

Rabgap1 knockout^(-/-) mice (C57BL/6N-Cr1-Rabgap1^{tm1b}(EUCOMM)HMGU/Jeg) were generated through allele conversion of C57BL/6N-Rabgap1^{tm1a}(EUCOMM)HmgU/Cnrm mouse line originating from The European Conditional Mouse Mutagenesis Program's embryonic stem cell clone, HEPD0553_3_H04. For further details on the construction of this clone, see the page at the International Mouse Phenotyping Consortium portal, <https://www.mousephenotype.org/data/genes/MGI:2385139>.

The tm1b allele was produced by deletion of exon 5 of *Rabgap1* and the neomycin cassette using a cell-permeable Cre recombinase.¹² This allele is considered a true knockout (KO) because skipping over of the LacZ cassette will not produce a functional protein. The cassette expresses LacZ under the control of the *Rabgap1* promoter as fusion protein with exon 4. For genotype analysis, genomic DNA was

extracted from tissue samples collected from mice during ear labeling at weaning age (3-weeks) and PCR was performed using *Rabgap1* specific primers (F *Rabgap1* 5' arm ctttgccctgcaatatgccat *Rabgp1*, 3' arm ggatttggccagagatga, and LAR3 caacgggttctctgttagtcc; expected size (base pairs [bp]) wild type: 645 bp and mutant: 513 bp). Heterozygous mice were intercrossed to generate homozygous mutants.

Mouse phenotyping

A cohort of 19 *Rabgap1*^{-/-} mice (10 males/9 females) and wild-type controls (22 males/26 females) underwent the early-adult screening pipeline at the German Mouse Clinic as partner institution of the International Mouse Phenotyping Consortium (<https://www.mousephenotype.org/>).^{12,13,14}

X-ray imaging was performed in an UltraFocus DXA system (Faxitron Bioptics, LLC) with automatic exposure control. To investigate a possible microcephaly in *Rabgap1* young mutant mice, X-ray images from 16-week-old female (5 controls and 5 *Rabgap1*^{-/-}) and male (5 controls and 4 *Rabgap1*^{-/-}) mice were analyzed using NDP.view2 software (Hamamatsu). In particular, we measured skull length (distance from the edge of the nasal bone until the first cervical vertebra) and width (distance representing maximum skull width across parietal bones). The relationship, in percentage, between skull length and width with body length was calculated. For statistical analyses, a Wilcoxon-Mann-Whitney test was applied to skull measurements.

For high throughput pathological analyses, we analyzed 4 *Rabgap1*^{-/-} mice (2 female/2 male) and 2 wild-type mice (1 female/1 male) at the age of 16 weeks. One additional *Rabgap1*^{-/-} female mouse was received for sectioning owing to welfare reasons at the age of 33 weeks. The mice were received for high throughput analysis, euthanized with carbon dioxide, and organs were analyzed macroscopically as described previously.^{15,16} For the histological analysis, hematoxylin and eosin staining of brains was performed on 4% buffered formalin-fixed paraffin-embedded sections (3 µm). Brains were analyzed using sagittal and limited serial coronal sections. The cut regions and positions were determined by Allen Mouse Brain Atlas (<https://mouse.brain-map.org/static/atlas>). In addition to routinely performed hematoxylin and eosin staining, brain sections were stained using Luxol fast blue for better visualization of myelinated tracts. Myelin/myelinated axons stained blue to green. The slides were analyzed by 2 independent pathologists.

For further experimental details, see [Supplemental Materials and Methods](#).

Results

Biallelic LOF variants in *RABGAP1*

Through GeneMatcher, we identified 5 patients internationally with homozygous variants in *RABGAP1*, inherited

from consanguineous heterozygous parents. All variants were identified through ES. In total, 3 different homozygous variants in *RABGAP1* were identified and all were predicted to result in loss of *RABGAP1* function (Figure 1A). Two of the variants affect canonical splice sites (NC_000009.12 [NM_012197.3]: c.591-1G>T detected in 2 siblings and c.1101+1del detected in 1 patient) and the third variant results in a premature stop codon (c.1072C>T; p.Arg358* detected in 2 siblings). All variants are upstream of both the TBC and the C-terminal coiled-coil domain in the *RABGAP1* protein. To validate an effect of the canonical splice site variants on splicing, LCLs were generated from one of the siblings carrying the c.591-1G>T variant and from her parents. We were not able to obtain cell lines from the other 2 patients with splice variants. RNA sequencing revealed a novel splicing event resulting in the loss of 8 base pairs from the 5' end of exon 5, predicted to result in a frameshift and premature stop codon (Figure 1B). This novel splicing event was also observed in the heterozygous parents. RNA sequencing results were validated through PCR by showing a decrease in the size of a PCR product spanning exons 4 and 5 (Figure 1C). When compared with internal controls and with the Genotype-Tissue Expression database, both proband and parents exhibited decreased RNA levels of *RABGAP1*, consistent with nonsense-mediated messenger RNA decay (Figure 1D). Of note, the parents are both healthy, have normal head circumferences, and have no neurodevelopmental challenges. In addition, ES identified several other variants in the patient cohort, which can be found in Supplemental Table 1.

Patients with biallelic LOF variants in *RABGAP1* present with microcephaly, global developmental delay, and multiple congenital anomalies

Clinical features of our cohort are summarized in Figure 1H. The patients' ages ranged from 2 to 13 years. All affected individuals with biallelic variants in *RABGAP1* presented with severe global developmental delay/intellectual disability. Significant microcephaly (on average, 3-4 SD below the mean) was present in all individuals except patient 4. In total, 4 patients had bilateral sensorineural hearing loss from birth. Two patients have a diagnosis of attention-deficit/hyperactivity disorder and one of the patients is pending further assessment for autism spectrum disorder. Prominent neurologic findings included congenital unilateral ptosis (1/5), exotropic strabismus (1/5), hypotonia (3/5), severe hypertonia and spasticity (2/5), hyperreflexia (3/5), and epilepsy (one patient with absence seizures; another patient with focal to generalized tonic-clonic seizures and episodes of status epilepticus). Notable overlapping craniofacial features included a beaked nose (4/5), micro-retrognathia (4/5), and synophrys (3/5) (Figure 1E, F, and H). Additional clinical features are detailed in Supplemental Table 1 and the Supplemental Note.

Neuroimaging shows delayed myelination and thinned corpus callosum in patients with biallelic LOF variants in *RABGAP1*

Neuroimaging results were reviewed for all patients. Delayed myelination, white matter volume loss, and thinning of the corpus callosum (Figure 1G) were seen in 4 of 5 patients. In addition, patient 4 had cortical atrophy of the right hemisphere after diffuse cortical swelling due to a prolonged episode of status epilepticus, a large cisterna magna, and severe ventriculomegaly with a distal aqueductal stenosis, requiring multiple ventriculostomies. Her presentation with profound ventriculomegaly, hydrocephaly, severe epilepsy, feeding difficulties, obesity (above +3 SD, World Health Organization body mass index-for-age girls), and absence of microcephaly (+1.3 SD) are unique to our cohort. It should be noted that she was found to have additional homozygous variants of uncertain significance in *FLVCR2* (NM_017791.3:c.452G>A p.Arg151His). Homozygous pathogenic variants in *FLVCR2* cause proliferative vasculopathy and hydranencephaly-hydrocephaly syndrome, also known as Fowler syndrome.¹⁷ Although she lacks the key features of proliferative vasculopathy and hydranencephaly-hydrocephaly syndrome (ie, absence of intracranial calcifications and abnormal vascular proliferations), it cannot be ruled out that these additional variants may be contributing to her phenotype.

Patient cells harboring biallelic variants in *RABGAP1* exhibit decreased mTOR signaling and abnormal lysosomal and endosomal positioning

Previous studies have revealed that a knockdown of *RABGAP1* in cells results in an abnormal localization of both lysosomal and endosomal compartments.¹¹ Cells with decreased *RABGAP1* were found to have a more dispersed appearance of both LAMP2 (which marks lysosomes and late endosomes) and early endosomal markers.¹¹ Examination of RAB5 (an early endosomal marker) localization in the LCLs revealed a significant increase in the number of cells with dispersed RAB5 staining in the affected patient and heterozygous parents when compared with a healthy control (Figure 2A). LAMP2 staining was also more distributed in the patient and their parents when compared with a healthy control although the patient also exhibited a significant increase when directly compared with their parents (Figure 2B). Overall, these findings are consistent with loss of *RABGAP1* function.

In addition, studies have shown that *RABGAP1* is required for mTORC1 activity, and *RABGAP1* knockdown in cells resulted in decreased phospho-S6 levels, a common readout for the mTOR pathway.¹¹ We measured the levels of both phospho-AKT (a readout for AKT signaling, a critical upstream kinase) and phospho-S6 in lymphoblastoid

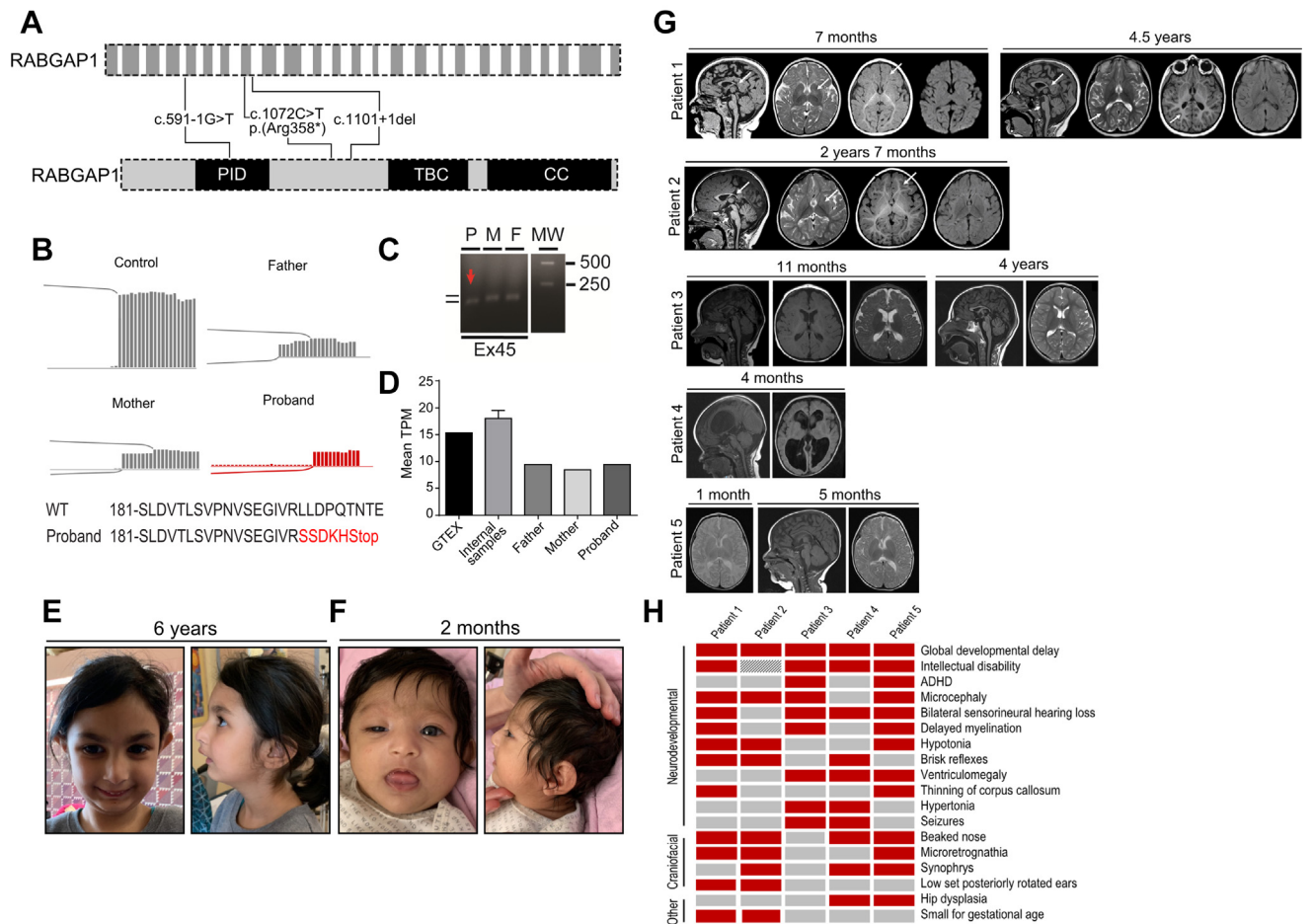


Figure 1 Biallelic variants in *RABGAP1* cause a novel neurodevelopmental syndrome. A. Schematic of the *RABGAP1* gene and *RABGAP1* protein with patient variants indicated. B. Sashimi plot denoting splice junctions at the 5' end of exon 5 in *RABGAP1* and resulting predicted protein sequence when the alternate junction is used. Human lymphoblastoid cell lines (LCLs) were generated from patient 1, her mother, and her father to perform RNA sequencing and analysis. C. Polymerase chain reaction products from primers spanning exon 4 and the middle of exon 5 showing the size of the product (red arrow) in the proband (patient 1) when compared with the M and F. The noticeably thicker bands in parent lanes (M and F) may be due to the presence of 2 poorly resolved bands that differ by only 8 base pair. MW of a ladder is also indicated. D. Comparison of mean transcripts per million for *RABGAP1* in the GTEx database, internal controls ($n = 6$), and patient 1 and her mother and father. E. Facial features, including a front and side profile of patient 1. F. Facial features, including a front and side profile of patient 2. G. Representative brain magnetic resonance imaging images from our patient cohort. Patient 1 at 7 months (from left to right): sagittal T1 shows a thin undermyelinated corpus callosum (arrow) tapering toward a hypoplastic splenium (arrow) and microcephaly. Axial T2 reveals incomplete, but age appropriate, myelin maturation of the white matter tracts (arrow) traversing the basal ganglia. Axial T1, however, shows delayed frontal lobe myelination (arrow). Diffusion weighted imaging is normal. Patient 1 at 4.5 years (from left to right): the dysgenetic shape of the corpus callosum (arrow) persists after myelin maturation on sagittal T1 image. The prepontine cistern (short arrow) has become mildly prominent, also suggesting relative thinning of the brainstem. Axial T2 and T1 weighted images reveal normal myelin maturation of the periarterial white matter (arrow) and peripheral white matter. The white matter volume is less than expected but has not decreased from the initial MRI at 7 months of age. Axial fluid-attenuated inversion recovery (FLAIR) shows normal signal. Patient 2 at 2 years 7 months (from left to right): the same configuration (arrow) of the corpus callosum is present on sagittal T1, despite satisfactory myelin maturation of the structure. The prepontine cistern is mildly prominent (short arrow), consistent with mild brainstem volume loss. Axial T2 now shows the low signal white matter tracts (arrow). Axial T1 shows progressive myelin maturation in the peripheral white matter (arrow) although the peripheral white matter tracts are thin for age. Axial FLAIR shows normal signal. Microcephaly is present, as is a mildly trigonocephalic head shape. Patient 3 at age 11 months. Shows white matter volume loss with delayed myelination that improved on subsequent imaging at 4 years. Patient 4 at 4 months. Reveals a large cisterna magna on T1 sagittal view and T2 images show severe ventriculomegaly and distal aqueductal stenosis (before third ventriculostomy). Patient 5 at 1 month. Shows thinning of the corpus callosum and absence of myelination of the posterior limb of the internal capsule (PLIC). At 5 months, there is myelination of the PLIC but no further myelination elsewhere. H. Summary of the clinical features found across the patient cohort. Note dashed lines through the box means the feature was not known or able to be diagnosed given the patient's age. ADHD, attention-deficit/hyperactivity disorder; CC, C-terminal coiled-coil domain; F, father; GTEx, Genotype-Tissue Expression; M, mother; MW, molecular weight; P, proband; PID, N-terminal phosphotyrosine interaction domain; TBC, TRE2/BUB2/CDC16 domain; WT, wild type.

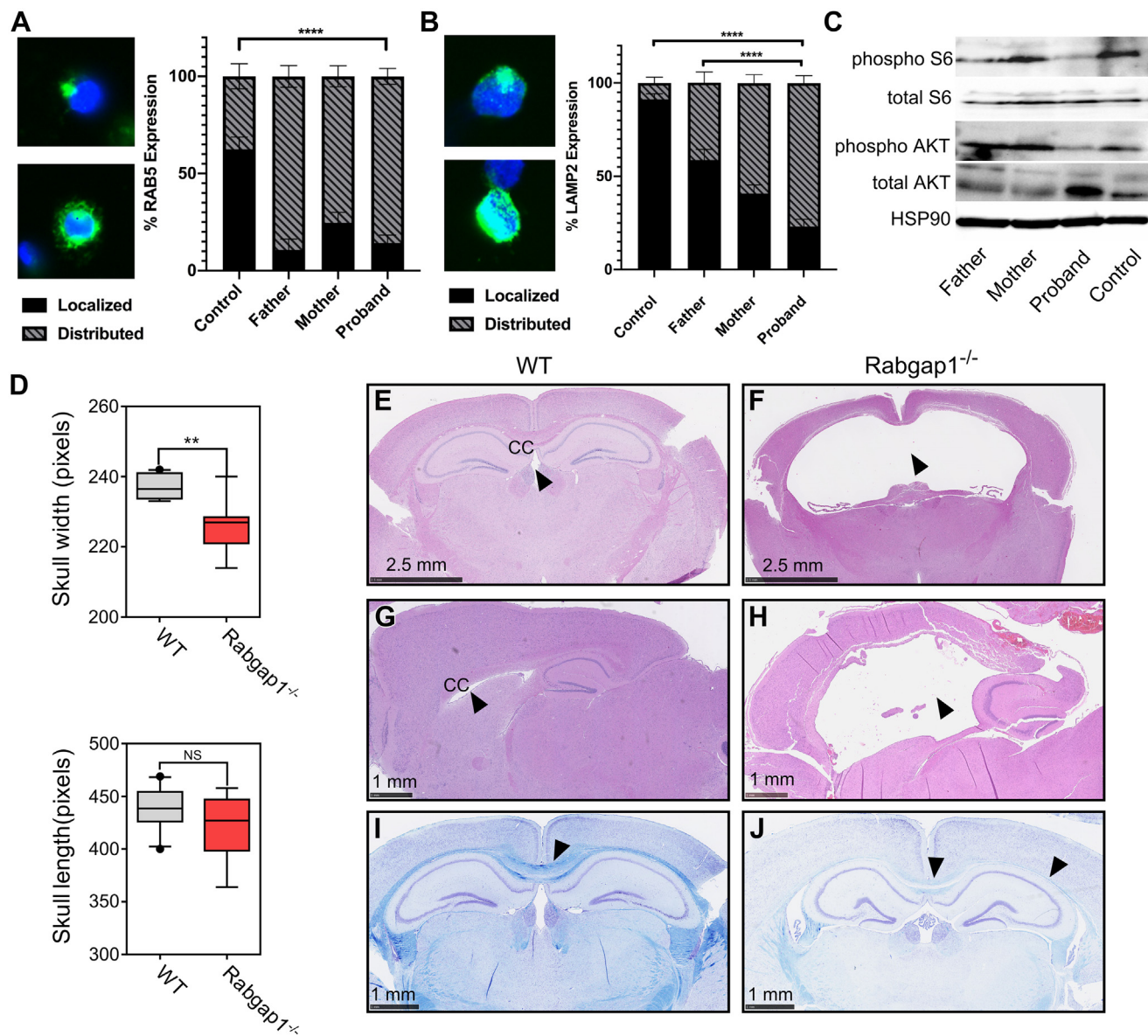


Figure 2 Characterization of patient 1's lymphoblastoid cell line and a mouse knockout model of *Rabgap1*. **A**, Comparison of percent of lymphoblastoid cells with either localized or distributed expression of RAB5 between a healthy control, proband (patient 1) and her parents ($****P < .0001$). **B**, Comparison of percent of lymphoblastoid cells with either localized or distributed expression of LAMP2 between a healthy control, proband (patient 1) and her parents ($****P < .0001$). **C**, Total S6, phospho S6, total AKT, and phospho AKT protein levels in a healthy control, proband, and her parents. pS6 and S6 are both 70 kDa. pAKT and AKT are both 60 kDa. HSP90 was used as a loading control (90 kDa). **D**, Skull width and skull length comparison between WT ($n = 10$) and *Rabgap1* knockouts ($n = 9$) ($**P < .05$). **E**, **F**, Coronal brain sections with hematoxylin and eosin (H&E) staining of a WT and a *Rabgap1* knockout mouse. CC denotes the corpus callosum, arrows indicate the normal ventricle in (F) and the dilated ventricle in (G). **G**, **H**, Sagittal brain sections with H&E staining of a WT and a *Rabgap1* knockout mouse. CC denotes the corpus callosum, arrows indicate the normal ventricle in (H) and the dilated ventricle in (I). **I**, **J**, Coronal brain sections with Toluidine blue staining of a WT and *Rabgap1* knockout mouse. Arrows indicate the corpus callosum. NS, not significant; WT, wild type.

cells derived from the proband, the parents, and a healthy control. Interestingly, there was decreased levels of both phospho-S6 and phospho-AKT in the proband when compared with either parent or the healthy control (Figure 2C). Altogether, our results are consistent with downregulated mTOR signaling in the patient cells, consistent with loss of RABGAP1.

***Rabgap1* KO mice also exhibit microcephaly, thinning of the corpus callosum, and ventriculomegaly**

Through GeneMatcher, we learned about a *Rabgap1* KO mouse model and were intrigued to find similar neurologic features as those seen in our patient cohort. During

macroscopic examination of the mice used for histopathology, 2 of 5 *Rabgap1* KO mice exhibited marked domed and thinned skull bones. X-ray images were analyzed and microcephaly, reflected in significantly reduced skull width, was diagnosed in mutant animals (Figure 2D). On histological analysis, 4 of 4 *Rabgap1* KO mice exhibited thinning of the corpus callosum whereas control, healthy mice had normal appearing corpora callosa (Figure 2I and J). The fifth *Rabgap1* KO mouse examined had such severe hydrocephalus with compressed tissue that the corpus callosum was not detectable. The mice with deformity of the skull also showed severe dilation of the third and lateral ventricles and atrophy of the cortex (2/5; Figure 2F and H). Hydrocephalus/ventriculomegaly has been reported in certain inbred strains of mice as a background feature (an incidence of 0.01-0.03% in the BL6 mice strain) and in genetically modified mice (with variable incidence).¹⁸ Given the low number of animals and patients in our cohort, it is difficult to conclude, without further studies of larger cohorts, whether ventriculomegaly is a hallmark feature.

Discussion

We provide evidence for a novel neurodevelopmental syndrome caused by biallelic LOF variants in *RABGAP1*. Variants in *RABGAP1* identified in our patient cohort are classified as pathogenic in accordance with American College of Medical Genetics and Genomics guidelines, fulfilling the criteria for pathogenicity with the following observations: not observed in large population databases (absent in Genome Aggregation Database); the 2 splice site variants are located in a canonical splice site, both of which are predicted to affect splicing *in silico*, and one of the splice site variants showed abnormal splicing that is predicted to result in a frameshift and premature stop codon (Figure 1B and C); the third variant results in a premature stop codon; the specific neurodevelopmental features shared by affected individuals from different families; and further supported by the similar phenotype seen in the *Rabgap1* KO mice.¹⁹ The mechanisms by which loss of *RABGAP1* result in the clinical features seen in our patients will require further investigation. mTOR signaling has been previously shown to be critical for brain development and a dysregulation in its signaling is associated with various neurodevelopmental and neuropsychiatric disorders.²⁰ Although there were some overlapping craniofacial abnormalities, including beaked nose, microretrognathia, and synophrys, it is difficult to conclude on a recognizable facial pattern with a small sample size. Of note, a similar constellation of craniofacial features and neurologic findings have been reported in a rare condition called Warburg micro syndrome or Maltsof syndrome (both due to *Rab18* deficiency caused by pathogenic variants in *RAB3GAP1*, *RAB3GAP2*, *RAB18*, or *TBC1D20*).^{21,22} However, our cohort lacked congenital

cataracts, microphthalmia, and hypogonadism, which are the hallmarks of *Rab18* deficiency although a wider phenotypic spectrum may exist as more cases are described. The reason for overlapping features may be explained by an indirect link between *RABGAP1* and *TBC1D20* as shown in a yeast 2-hybrid study, however further experimental studies will be required to test this hypothesis.²³

We present evidence that biallelic variants in *RABGAP1* lead to abnormal neurodevelopment through a LOF mechanism, which may be mediated by downregulation of the mTORC1 signaling pathway. We propose the term *RABGAP1*-related disorder to describe this condition associated with neurodevelopmental and multiple congenital anomalies caused by pathogenic *RABGAP1* variants.

Data Availability

Clinical data and materials will be shared upon request to the corresponding author.

Acknowledgments

We are grateful to the patients and their families for their participation in the development of this case series. K.E.Y. was supported by a Genome Canada Disruptive Innovation in Genomics grant (OGI-158) to J.D. and M.D.W. *Rabgap1* knock out mouse phenotyping was supported by German Federal Ministry of Education and Research (Infrafrontier grant 01KX1012 to M.H.d.A.) and German Center for Diabetes Research (DZD) (to M.H.d.A.).

Author Information

Conceptualization: R.Y.O., A.R.D., A.M., J.D., A.S., T.K.-R., J.C.-W., A.S.-M., M.K., S.M., H.F., V.G.-D., M.H.d.A.; Data Curation: R.Y.O., A.R.D., A.M., N.S., M.T., H.H., K.E.Y., M.D.W., P.R., R.L., N.E., C.W.T.C., S.H., T.K.-R., J.C.-W., A.S.-M., M.K., S.M., H.F., V.G.-D., M.H.d.A., J.D., A.S.; Formal Analysis: R.Y.O., A.R.D., N.S., M.T., H.H., K.E.Y., M.D.W., T.K.-R., J.C.-W., A.S.-M., M.K., S.M., H.F., V.G.-D., M.H.d.A.; Funding Acquisition: M.D.W., J.D., A.S., M.H.d.A.; Investigation: R.Y.O., A.R.D., A.M., P.R., R.L., N.E., C.W.T.C., S.H., T.K.-R., J.C.-W., A.S.-M., M.K., S.M., H.F., V.G.-D., M.H.d.A.; Methodology: A.R.D., N.S., M.T., H.H., K.E.Y., M.D.W., T.K.-R., J.C.-W., A.S.-M., M.K., S.M., H.F., V.G.-D., M.H.d.A., A.R.D., A.S.; Project Administration: R.Y.O., A.R.D., A.S., M.H.d.A., H.F., V.G.-D.; Resources: M.D.W., A.S.-M., H.F., V.G.-D., M.H.d.A., J.D., A.S.; Software: T.K.-R., A.S.-M., H.F., V.G.-D.; Supervision: M.H.d.A., J.D., M.D.W., A.S.; Validation:

A.R.D., N.S., M.T., H.H., K.E.Y., M.D.W., T.K.-R., J.C.-W., A.S.-M., M.K., S.M., H.F., V.G.-D.; Visualization: R.Y.O., A.R.D., A.M., M.T., A.S.; Writing-original draft: R.Y.O., A.R.D.; Writing-review and editing: R.Y.O., A.R.D., A.M., M.D.W., P.R., R.L., N.E., C.W.T.C., T.K.-R., J.C.-W., A.S.-M., H.F., V.G.-D., A.S.

Ethics Declaration

Written informed consents were obtained from families for the publication of clinical information and photos. Consent for functional studies on generated lymphoblastoid cell lines from our patient (patient 1) and her parents were also obtained through the Care4Rare phase 2 study. Mice were maintained in individually ventilated cages with water and standard mouse chow according to the directive 2010/63/EU, German laws, and German Mouse Clinic housing conditions (www.mouseclinic.de). Experimental procedures were approved by the responsible authority of the district government of Upper Bavaria, Germany.

Conflict of Interest

The authors declare no conflict of interest.

Additional Information

The online version of this article (<https://doi.org/10.1016/j.gim.2022.07.024>) contains supplementary material, which is available to authorized users.

Affiliations

¹Division of Clinical and Metabolic Genetics, The Hospital for Sick Children, Toronto, Ontario, Canada; ²Program in Genetics and Genome Biology, Hospital for Sick Children, Toronto, Ontario, Canada; ³Department of Medical Genetics, University of Calgary, Calgary, Alberta, Canada; ⁴Department of Genetics, University Medical Center Groningen, University of Groningen, Groningen, the Netherlands; ⁵Department of Clinical Genetics, Liverpool Hospital, Sydney, New South Wales, Australia; ⁶School of Women's and Children's Health, University of New South Wales, Sydney, New South Wales, Australia; ⁷German Mouse Clinic, Institute of Experimental Genetics, Helmholtz Zentrum München, German Research Center for Environmental Health (GmbH), Ingolstaedter Landstraße, Neuherberg, Germany; ⁸Chair of Experimental Genetics, TUM School of Life Sciences, Technische Universität

München, Freising, Germany; ⁹German Center for Diabetes Research (DZD), Ingolstaedter Landstraße, Neuherberg, Germany; ¹⁰Division of Neurology, The Hospital for Sick Children, Toronto, Ontario, Canada; ¹¹Departments of Paediatrics and Biochemistry, University of Toronto, Toronto, Ontario, Canada

References

1. Cuif MH, Possmayer F, Zander H, et al. Characterization of GAPCenA, a GTPase activating protein for Rab6, part of which associates with the centrosome. *EMBO J*. 1999;18(7):1772-1782. <http://doi.org/10.1093/emboj/18.7.1772>
2. Opdam FJ, Echard A, Croes HJ, et al. The small GTPase Rab6B, a novel Rab6 subfamily member, is cell-type specifically expressed and localised to the Golgi apparatus. *J Cell Sci*. 2000;113(Pt 15):2725-2735. <http://doi.org/10.1242/jcs.113.15.2725>
3. Kanno E, Ishibashi K, Kobayashi H, Matsui T, Ohbayashi N, Fukuda M. Comprehensive screening for novel rab-binding proteins by GST pull-down assay using 60 different mammalian Rabs. *Traffic*. 2010;11(4):491-507. <http://doi.org/10.1111/j.1600-0854.2010.01038.x>
4. Frasa MAM, Koessmeier KT, Ahmadian MR, Braga VMM. Illuminating the functional and structural repertoire of human TBC/RABGAPs. *Nat Rev Mol Cell Biol*. 2012;13(2):67-73. Published correction appears in *Nat Rev Mol Cell Biol*. 2012;13(7):476. <https://doi.org/10.1038/nrm3267>
5. Goud B, Zahraoui A, Tavitian A, Saraste J. Small GTP-binding protein associated with Golgi cisternae. *Nature*. 1990;345(6275):553-556. <http://doi.org/10.1038/345553a0>
6. Antony C, Cibert C, Géraud G, et al. The small GTP-binding protein rab6p is distributed from medial Golgi to the trans-Golgi network as determined by a confocal microscopic approach. *J Cell Sci*. 1992;103(Pt 3):785-796. <http://doi.org/10.1242/jcs.103.3.785>
7. Martinez O, Antony C, Pehau-Arnaudet G, Berger EG, Salamero J, Goud B. GTP-bound forms of rab6 induce the redistribution of Golgi proteins into the endoplasmic reticulum. *Proc Natl Acad Sci U S A*. 1997;94(5):1828-1833. <http://doi.org/10.1073/pnas.94.5.1828>
8. Girod A, Storrie B, Simpson JC, et al. Evidence for a COP-I-independent transport route from the Golgi complex to the endoplasmic reticulum. *Nat Cell Biol*. 1999;1(7):423-430. <http://doi.org/10.1038/15658>
9. White J, Johannes L, Mallard F, et al. Rab6 coordinates a novel Golgi to ER retrograde transport pathway in live cells. *J Cell Biol*. 1999;147(4):743-760. Published correction appears in *J Cell Biol*. 2000;148(1):205. <https://doi.org/10.1083/jcb.147.4.743>
10. Mallard F, Tang BL, Galli T, et al. Early/recycling endosomes-to-TGN transport involves two SNARE complexes and a Rab6 isoform. *J Cell Biol*. 2002;156(4):653-664. <http://doi.org/10.1083/jcb.200110081>
11. Kawasaki N, Isogaya K, Dan S, et al. TUFT1 interacts with RABGAP1 and regulates mTORC1 signaling. *Cell Discov*. 2018;4(1):1. <http://doi.org/10.1038/s41421-017-0001-2>
12. Ryder E, Doe B, Gleeson D, et al. Rapid conversion of EUCCOMM/KOMP-CSD alleles in mouse embryos using a cell-permeable Cre recombinase. *Transgen Res*. 2014;23(1):177-185. <http://doi.org/10.1007/s11248-013-9764-x>
13. Gailus-Dumer V, Fuchs H, Becker L, et al. Introducing the German Mouse Clinic: open access platform for standardized phenotyping. *Nat Methods*. 2005;2(6):403-404. <http://doi.org/10.1038/nmeth0605-403>
14. Fuchs H, Aguilar-Pimentel JA, Amarie OV, et al. Understanding gene functions and disease mechanisms: phenotyping pipelines in the German Mouse Clinic. *Behav Brain Res*. 2018;352:187-196. <http://doi.org/10.1016/j.bbr.2017.09.048>
15. Parmenter MD, Gray MM, Hogan CA, et al. Genetics of skeletal evolution in unusually large mice from Gough Island. *Genetics*. 2016;204:1559-1572. <http://doi.org/10.1534/genetics.116.193805>

16. Fuchs H, Gailus-Dumer V, Adler T, et al. Mouse phenotyping. *Methods*. 2011;53:120-135. <http://doi.org/10.1016/j.ymeth.2010.08.006>
17. Kvarnung M, Taylan F, Nilsson D, et al. Mutations in FLVCR2 associated with Fowler syndrome and survival beyond infancy. *Clin Genet*. 2016;89(1):99-103. <http://doi.org/10.1111/cge.12565>
18. Sundberg JP, Woolcott BL, Cunliffe-Beamer T, Brown KS, Bronson R. Spontaneous hydrocephalus in inbred strains of mice. The Jackson Laboratory. Published April 01, 1991. Accessed July 15, 2022. <https://www.jax.org/news-and-insights/1991/april/spontaneous-hydrocephalus-in-inbred-strains-of-mice>
19. Richards S, Aziz N, Bale S, et al. Standards and guidelines for the interpretation of sequence variants: A joint consensus recommendation of the American College of Medical Genetics and Genomics and the association for molecular pathology. *Genet Med*. 2015;17(5):405-424. <http://doi.org/10.1038/gim.2015.30>
20. Costa-Mattioli M, Monteggia LM. mTOR complexes in neurodevelopmental and neuropsychiatric disorders. *Nat Neurosci*. 2013;16(11):1537-1543. <http://doi.org/10.1038/nn.3546>
21. Handley MT, Morris-Rosendahl DJ, Brown S, et al. Mutation spectrum in RAB3GAP1, RAB3GAP2, and RAB18 and genotype-phenotype correlations in Warburg micro syndrome and Martsolf syndrome. *Hum Mutat*. 2013;34(5):686-696. <http://doi.org/10.1002/humu.22296>
22. Imagawa E, Fukai R, Behnam M, et al. Two novel homozygous RAB3GAP1 mutations cause Warburg micro syndrome. *Hum Genome Var*. 2015;2:15034. <http://doi.org/10.1038/hgv.2015.34>
23. Davey JR, Humphrey SJ, Junutula JR, et al. TBC1D13 is a RAB35 specific GAP that plays an important role in GLUT4 trafficking in adipocytes. *Traffic*. 2012;13(10):1429-1441. <http://doi.org/10.1111/j.1600-0854.2012.01397.x>